



**HAL**  
open science

## Chip-Scale Terahertz Frequency Combs through Integrated Intersubband Polariton Bleaching

Francesco P Mezzapesa, Leonardo Viti, Lianhe Li, Valentino Pistore,  
Sukhdeep Dhillon, A. Giles Davies, Edmund H Linfield, Miriam S Vitiello

► **To cite this version:**

Francesco P Mezzapesa, Leonardo Viti, Lianhe Li, Valentino Pistore, Sukhdeep Dhillon, et al.. Chip-Scale Terahertz Frequency Combs through Integrated Intersubband Polariton Bleaching. *Laser and Photonics Reviews*, 2021, pp.2000575. 10.1002/lpor.202000575 . hal-03230729

**HAL Id: hal-03230729**

**<https://hal.sorbonne-universite.fr/hal-03230729>**

Submitted on 20 May 2021

**HAL** is a multi-disciplinary open access archive for the deposit and dissemination of scientific research documents, whether they are published or not. The documents may come from teaching and research institutions in France or abroad, or from public or private research centers.

L'archive ouverte pluridisciplinaire **HAL**, est destinée au dépôt et à la diffusion de documents scientifiques de niveau recherche, publiés ou non, émanant des établissements d'enseignement et de recherche français ou étrangers, des laboratoires publics ou privés.

# Chip-Scale Terahertz Frequency Combs through Integrated Intersubband Polariton Bleaching

Francesco P. Mezzapesa, Leonardo Viti, Lianhe Li, Valentino Pistore, Sukhdeep Dhillon, A. Giles Davies, Edmund H. Linfield, and Miriam S. Vitiello\*

Quantum cascade lasers (QCLs) represent a fascinating accomplishment of quantum engineering and enable the direct generation of terahertz (THz) frequency radiation from an electrically biased semiconductor heterostructure. Their large spectral bandwidth, high output powers, and quantum-limited linewidths have facilitated the realization of THz pulses by active mode-locking and passive generation of optical frequency combs (FCs) through intracavity four-wave-mixing, albeit over a restricted operational regime. Here, an integrated architecture is conceived for the generation of high power (5.5–8.0 mW) THz FCs comprising an ultrafast THz polaritonic reflector, exploiting intersubband (ISB) cavity polaritons, and a broad bandwidth (2.3–3.8 THz) heterogenous THz QCL. By tuning the group-delay-dispersion in an integrated geometry, through the exploitation of light-induced bleaching of the ISB-based THz polaritons, spectral reshaping of the QCL emission and stable FC operation over an operational range up to 38%, characterized by a single and narrow (down to 700 Hz) intermode beatnote are demonstrated. This concept provides design guidelines for a new generation of compact, cost-effective, electrically driven chip-scale FC sources based on ultrafast polariton dynamics, paving the way toward the generation of mode-locked THz microlasers that can strongly impact a broad range of applications in ultrafast sciences, data storage, high-speed communication, and spectroscopy.

nanoscale, for quantum metrology,<sup>[2]</sup> for communications,<sup>[3]</sup> and for multiplexed analysis of gas samples requiring narrow-linewidth and a tight control of frequency jitter.<sup>[4]</sup> The most common technique to generate an FC in a solid-state laser is through mode-locking:<sup>[5,6]</sup> the longitudinal modes of the laser cavity are locked in phase by means of an external (active) or internal (self- or passive) modulation mechanism, giving rise to a train of equidistant and intense pulses with a repetition rate equal to the inverse cavity round-trip time. Although mode-locked lasers have been widely demonstrated in the visible and near-infrared frequency ranges,<sup>[5,7]</sup> engineering passively mode-locked lasers in a compact and miniaturized architecture, across the THz frequency region of the electromagnetic spectrum, remains elusive.

Quantum cascade lasers (QCLs) have become, in the last decade, the most prominent electrically driven source of THz radiation, owing to their inherently high quantum efficiency,<sup>[8,9]</sup> compactness, and spectral purity.<sup>[10]</sup> There is a fundamental obstacle preventing mode-locking with passive generation of ultra-short pulses in the semiconductor gain medium of a THz QCL: owing to the intersubband (ISB) architecture, the carrier relaxation is extremely fast (5–10 ps).<sup>[11]</sup> As such, the gain recovery time is shorter than the cavity round-trip time ( $\approx 70$  ps for a 3 mm cavity),<sup>[12]</sup> complicating the generation of stable ultrafast laser pulses.

## 1. Introduction


The generation of stable frequency comb (FC) synthesizers with large optical powers per comb tooth,<sup>[1]</sup> at terahertz (THz) frequencies (wavelength 300–30  $\mu\text{m}$ ), is fundamental for the investigation of light–matter interaction phenomena at the

Dr. F. P. Mezzapesa, L. Viti, Prof. M. S. Vitiello  
NEST  
CNR - Istituto Nanoscienze and Scuola Normale Superiore  
Piazza San Silvestro 12, Pisa 56127, Italy  
E-mail: miriam.vitiello@sns.it

Dr. L. Li, Prof. A. G. Davies, Prof. E. H. Linfield  
School of Electronic and Electrical Engineering  
University of Leeds  
Leeds LS2 9JT, UK

Dr. V. Pistore, Dr. S. Dhillon  
Laboratoire de Physique de l'Ecole Normale Supérieure  
Université PSL, CNRS, Sorbonne Université, Université de Paris  
Paris F-75005, France

Dr. V. Pistore  
NEST  
CNR - Istituto Nanoscienze and Scuola Normale Superiore  
Piazza San Silvestro 12 Pisa 56127, Italy

 The ORCID identification number(s) for the author(s) of this article can be found under <https://doi.org/10.1002/lpor.202000575>

© 2021 The Authors. Laser & Photonics Reviews published by Wiley-VCH GmbH. This is an open access article under the terms of the Creative Commons Attribution License, which permits use, distribution and reproduction in any medium, provided the original work is properly cited.

DOI: 10.1002/lpor.202000575

However QCLs, with specially designed heterogenous<sup>[13–16]</sup> or homogenous<sup>[17]</sup> active regions (ARs), can perform as chip-scale THz FCs, characterized, in the frequency domain, by a set of equidistant spectral lines, which share a well-defined and stable phase relationship between one another. This is enabled by the large third-order nonlinear susceptibility of the active medium, which gives rise to the interaction between adjacent modes via four wave mixing (FWM)<sup>[18,19]</sup> that generally results in a frequency modulated FC, i.e., a quasi-continuous wave (CW) output. In a THz QCL, the behavior is, in reality, more complex where both frequency and amplitude modulation are generally present,<sup>[20]</sup> and act simultaneously.

One of the major drawbacks of THz QCL FCs is that the bias-dependent group delay dispersion (GDD) usually compromises phase-locking of the laser modes over most of the laser operational range, therefore requiring proper dispersion compensation strategies. Successful approaches, commonly adopted in homogenous FCs, include waveguide re-shaping,<sup>[15]</sup> or integration with biased external elements.<sup>[21]</sup> Coupling with an unbiased external gold mirror has been conversely adopted to modify the reflectivity of heterogenous FCs,<sup>[22]</sup> providing dispersion compensation, although only over a limited portion of the QCL operational bandwidth. Dispersion is indeed very complex in heterogenous THz QCLs and a simple metallic mirror cannot compensate the GDD over the entire laser bandwidth.

Semiconductor mirrors, relying on inherently fast ISB polariton dynamics, could be in principle ideal, in this respect. They simultaneously provide an easier self-integration in the QCL cavity, while still maintaining a significant flexibility in terms of design and spectral bandwidth. Furthermore, recently, we have demonstrated that by strong coupling of ISB transitions<sup>[23,24]</sup> of semiconductor quantum wells to the photonic mode of a metallic cavity, we can custom tailor the population and polarization dynamics of ISB cavity polaritons in the saturation regime.<sup>[25,26]</sup> This results in efficient solid-state mirrors operating in the 2–3 THz range<sup>[25,26]</sup> that can provide a strong modulation of the optical response on sub-cycle timescales, accompanied by a recovery time  $\approx 3.3$  ps.

In the present work, we conceive an all-solid-state architecture in which the polaritonic mirror is integrated with a set of broadband heterogenous THz QCLs, having dissimilar dimensions. We first match the polaritonic doublet with the heterogenous QCL bandwidth. Then, by exploiting the complex reflectivity change associated with the light-induced bleaching of ISB polaritons, we tune the GDD, achieving compensation over a bandwidth and a current range much larger than that reached so far in any bare THz QCL FC. The fabricated devices show stable operation as optical FCs over an operational range  $> 35\%$ , significantly larger than that spontaneously achievable (12%–15%) from the corresponding bare QCL.<sup>[14]</sup> They deliver up to 8 mW of CW output power, with ultra-narrow (760 Hz) intermode beatnote linewidths (LWs), and  $> 80$  equally spaced optical modes, covering a maximum bandwidth of 0.85 THz in the comb regime and of 1.5 THz in the dispersion dominated regime. Furthermore, we show that the integrated polaritonic mirror can reshape the QCL emission spectrum leading to a significant mode proliferation at half of the laser operational range (i.e., current density  $J = 1.43 J_{\text{th}}$ , where  $J_{\text{th}}$  is the threshold current density), with a corresponding narrow intermode beat-

note. This is the signature of phase locking of the laser modes in a regime where the heterogenous nature of the gain media spontaneously entangles the dispersion dynamics.

## 2. Experimental Results

### 2.1. Samples Description, Experimental Setups, and Simulations

The polaritonic mirror is based on a semiconductor multi-quantum-well (MQW) heterostructure, resonant at the ISB transition frequency  $\nu_{\text{ISB}} = 2.7$  THz<sup>[25,26]</sup> having a doping concentration of  $1.0 \times 10^{10}$  cm<sup>-2</sup> charge carriers per QW, carefully optimized to achieve an optically pumping-induced reflectivity change (polaritonic bleaching) at reasonably low pump intensities  $I_p \sim 11$  W cm<sup>-2</sup>.<sup>[26]</sup> The MQW stack is embedded in an  $\approx 2$   $\mu\text{m}$  cavity, consisting of a back Au reflector and a top Au grating with period 16  $\mu\text{m}$ . The latter provides the required optical coupling to the MQW. When radiation polarized orthogonal to the grating lines (p-polarization) impinges at normal incidence, a fringe electric field is localized within the MQW heterostructure at the metallic edges of the grating. This field distribution satisfies the ISB transition selection rule in the near-field via the nonvanishing component  $E_z$  along the MQW growth direction.<sup>[26]</sup>

The reflectance of the polaritonic mirror, measured in vacuum at low temperature (6 K) for normal incidence (Figure 1a), reveals a characteristic polaritonic doublet<sup>[27]</sup> separated by a Rabi frequency of 0.18 THz. We exploit the ultrastrong light–matter coupling of the designed ISB transition (black curve Figure 1a) to the near-field of the metallic grating; the strong field enhancement induced by the reduced mode volume significantly enhances the optical absorption when compared to the bare electronic transition, therefore leading to a reduced saturation power in the two-state polaritonic system. By pumping the polaritonic mirror with a CW, 2.75 THz laser, we observe a spectral change of the reflectivity at intensities larger than 7.8 W cm<sup>-2</sup>, reflected in the bleaching of the upper polaritonic mode.<sup>[26]</sup> This results in a visible reflectivity change in the 2–3 THz spectral window, as shown in Figure 1a, where three prototypical reflectivity curves, corresponding to driving currents of the incident QCL of 520, 580, and 632 mA, are shown.

Such an effect can be innovatively exploited to tailor the intracavity dynamics of broadband QCLs by modifying their cavity dispersion. To this end, we use the polaritonic mirror as the back mirror of a set of free-running THz QCL FCs (Figure 1b), exploiting two different heterogenous ARs, which allow broadband operation over a bandwidth (2.3–3.8 THz) that matches, on its low frequency side, the spectral position of the polaritonic doublet (Figure 1a). This ensures that the reflectivity spectrum of the polaritonic doublet partially overlaps with the gain profile of the QCLs used (Figure 1c). The variation of the peak value of the gain profile is used in the simulations to reproduce the increase of the dispersion for higher currents, which occurs even though the maximum gain is clamped to the total losses.<sup>[28]</sup>

The two GaAs/AlGaAs QCL heterostructures each comprise three active modules, exploiting alternating photon- and longitudinal optical (LO) phonon-assisted interminiband transitions,<sup>[29]</sup> individually designed to operate at a different central frequency (2.5, 3.0, 3.5 THz). The two ARs differ in the doping concentration ( $n_d = 3.2 \times 10^{16}$  cm<sup>-3</sup> for laser A, and  $n_d = 4.0 \times 10^{16}$  cm<sup>-3</sup>

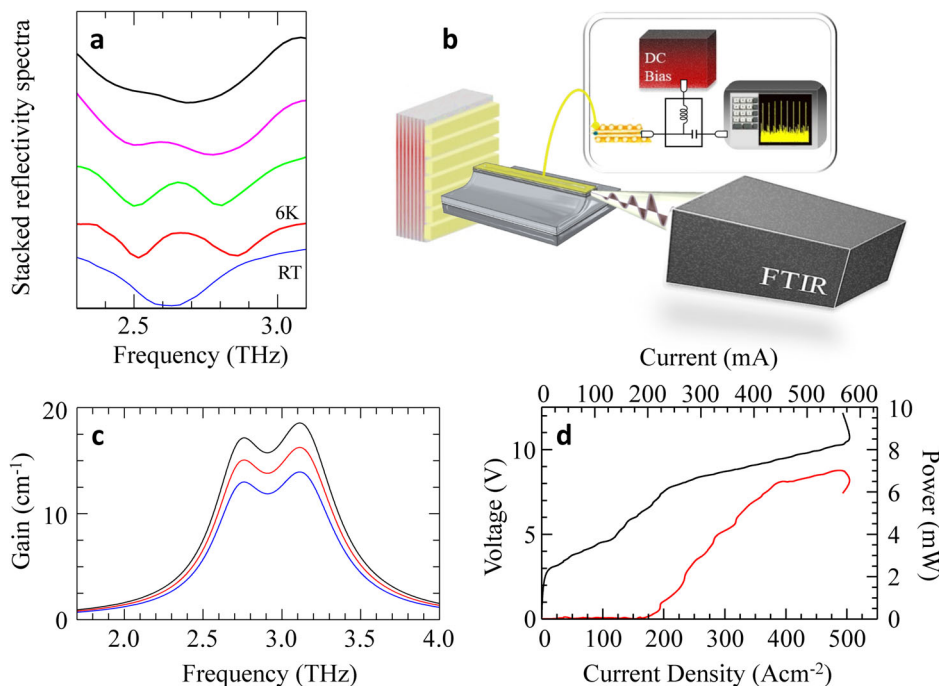


**Figure 1.** a) Reflectivity spectra of the polaritonic structure measured at  $T = 300$  K (blue curve), and at  $T = 6$  K while pumping on it a continuous-wave QCL (laser A) driven at  $I = 0$  mA (red curve),  $I = 520$  mA (green curve),  $I = 580$  mA (pink curve),  $I = 632$  mA (black curve). b) Schematic diagram showing the experimental arrangement. c) Gain profile of laser A, extrapolated from the corresponding experimental emission spectra collected at driving currents  $I_A = 520$  mA;  $I_A = 580$  mA;  $I_A = 632$  mA (from bottom to top). d) LJV characteristics of laser B. Analogous plots for laser A are reported in ref. [14].

for laser B), which is optimized to achieve a flat gain bandwidth (Figure 1c for laser A) and uniform power output across the whole spectrum, and to obtain two equivalently high dynamic ranges of current density, defined as the ratio between the maximum current density ( $J_{\max}$ ) and the threshold current density ( $J_{\max}/J_{\text{th}} = 2.9$ ). Both lasers are fabricated in a metal-metal waveguide configuration with a set of nickel side absorbers<sup>[14]</sup> that have the specific purpose of inhibiting lasing from higher order lateral modes. Laser A is  $85 \mu\text{m}$  wide and  $2.9$  mm long, laser B is  $50 \mu\text{m}$  wide and  $2.3$  mm long. The comparison between the light-current density-voltage (LJV) characteristics of laser A<sup>[14]</sup> and B (Figure 1d) reveals a doping-dependent threshold current density increase, varying from  $150 \text{ A cm}^{-2}$  in sample A, to  $175 \text{ A cm}^{-2}$  in sample B.

The polaritonic mirror is mounted, together with the QCL, on the copper cold-unit of a helium-flow cryostat and tightly coupled to the QCL back-facet at a distance  $d_c \sim 50 \pm 2 \mu\text{m}$ , determined by a fixed spacer. This defines a Gires-Tournois interferometer (GTI) created by the external cavity between the QCL back-facet and the surface of the polaritonic sample,<sup>[30,22]</sup> which is intentionally predefined to create a chromatic dispersion opposite to that arising in the QCL cavity, within the frequency range of interest. The polaritonic grating is oriented in a direction orthogonal to the QCL light polarization axis (p-polarization) to excite the MQW ISB transitions.

To show the effect of dispersion compensation from the polaritonic mirror, we perform numerical simulations of the GDD (see the Supporting Information). The frequency-dependent and QCL driving-current-dependent reflectivity change provided by the polaritonic mirror plays a major role in compensating dis-

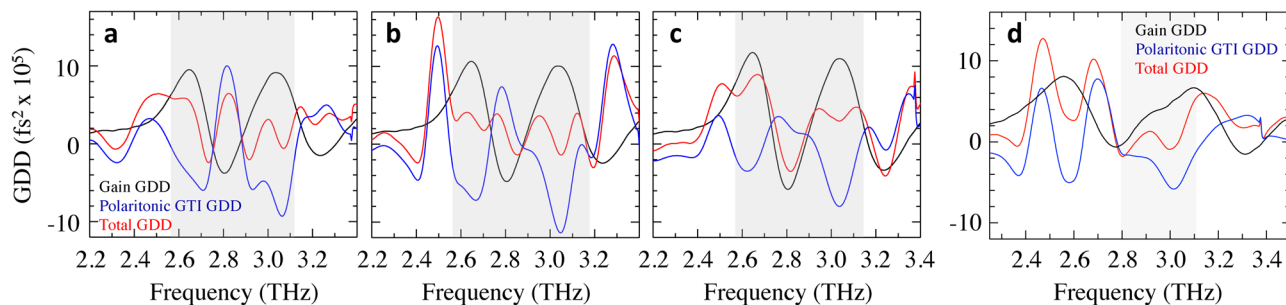
persion over a broader spectral window with respect to what demonstrated so far with a standard GTI comprising a gold mirror.<sup>[22]</sup>

Figure 2a–c shows the dispersion profiles due to the gain and the material (in black), the GTI with the polaritonic mirror (in blue), and the sum of all the contributions (in red), calculated at different driving currents, for laser A. The reduction of the overall dispersion was evaluated by computing the average of the absolute value of the dispersion profiles in the lasing range ( $2.55$ – $3.25$  THz). Without the GTI, the average dispersion due to the gain and the material increases from  $4.99 \times 10^5 \text{ fs}^2$  at  $I_A = 520$  mA to  $5.58 \times 10^5 \text{ fs}^2$  at  $I_A = 580$  mA, and then to  $6.18 \times 10^5 \text{ fs}^2$  at  $I_A = 632$  mA. By employing a GTI, the average dispersion is  $3.03 \times 10^5 \text{ fs}^2$  at  $I_A = 520$  mA,  $2.27 \times 10^5 \text{ fs}^2$  at  $I_A = 580$  mA, and  $4.11 \times 10^5 \text{ fs}^2$  at  $I_A = 632$  mA. The driving current where the lowest dispersion is achieved is  $\approx 580$  mA; that is also where the LW of the experimentally measured beatnote approaches  $700$  Hz.

We then run a further set of simulations while driving laser A at higher currents. Figure 2d shows the simulation results at  $I_A = 800$  mA. As clearly visible from the plot, the polaritonic GTI is unable to compensate or even significantly reduce dispersion, except in a small spectral window ( $2.8$ – $3.1$  THz), with a visible major GDD increase at frequencies  $< 2.8$  THz, meaning that no major effects on the QCL mode behavior is expected in such a biasing regime.

### 3. Results and Discussion

The QCLs are electrically driven in CW at a heat sink temperature  $T_{\text{H}} = 15$  K, over a bias-tee, which allows the free running



**Figure 2.** a–d) Simulated group delay dispersions (GDDs): GDD of the QCL gain (black curve), GDD of the polaritonic mirror (blue curve), and total GDD (red curve) of the resulting GTI calculated for a GTI length of 50  $\mu\text{m}$  when the QCL is driven with a current a)  $I_A = 520$  mA, b)  $I_A = 580$  mA, c)  $I_A = 632$  mA, and d)  $I_A = 800$  mA. The shaded gray areas mark the spectral regime in which the total GDD remains lower than the QCL GDD, leading to a–c) GDD compensation or d) to a negligible effect on the overall GDD.

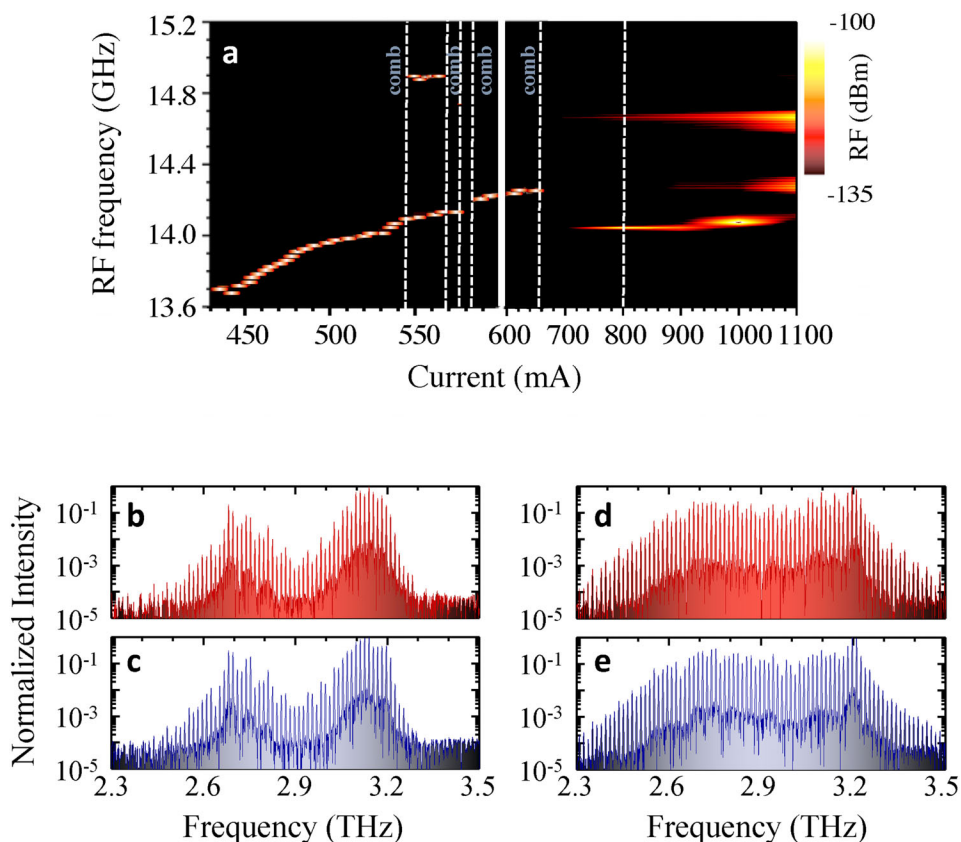


**Figure 3.** Laser A. Spectral characterization and intermode beatnote spectroscopy. a) Electrical RF intermode beatnote map measured at 15 K, as a function of the QCL bias current for a 2.9 mm long, 85  $\mu\text{m}$  wide laser bar coupled at a distance  $d_c = 50$   $\mu\text{m}$  to a polaritonic saturable absorber mirror; b–e) FTIR emission spectra collected at 15 K, while driving the QCL in CW at b,c)  $I_A = 650$  mA and d,e) at  $I_A = 800$  mA in the coupled b,d) QCL-polaritonic mirror system and in the c,e) bare laser A, respectively.

electrical beatnote of the QCL combs to be monitored using an radio frequency (RF) spectrum analyzer (*R&S FSW43*). The output radiation is aligned with an in-vacuum Fourier transform infrared spectrometer (FTIR, Bruker Vertex 80v), with a resolution of 0.075  $\text{cm}^{-1}$ . Under this experimental configuration, we can simultaneously record the output THz spectrum of the sources and their RF power spectral density.

We first test the operation of the polaritonic mirror by coupling it to laser A,<sup>[14]</sup> which naturally behaves like a comb in

the current ranges  $I_A = 430\text{--}536$  mA and  $540\text{--}543$  mA.<sup>[14]</sup> The multimode THz spectrum consists of equidistant modes, which beat together, causing a modulation of the laser intensity at a frequency in the range 13.7–14.0 GHz. We span the operation current of the laser A ( $I_A$ ) over the whole dynamic current range ( $\Delta I_A = 670$  mA) while collecting the intermode beatnote and the corresponding FTIR emission spectra.

**Figure 3a** shows the intermode beatnote map of the coupled system, as a function of  $I_A$ . A single beatnote is observed in a

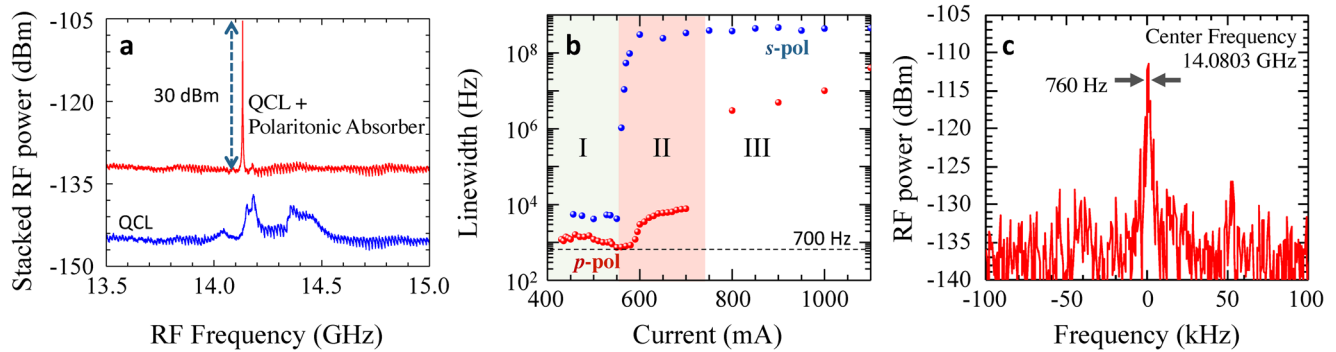


**Figure 4.** a) Stacked electrical intermode beatnotes acquired at  $T_H = 15$  K, while driving the bare laser A and the same laser coupled with the polaritonic mirror at driving currents of 650 mA. The RF spectra have been shifted vertically by 15 dBm. b) Intermode beatnote linewidth of laser A coupled with the polaritonic mirror under p-polarization (red) or s-polarization (blue), plotted as a function of the driving current. The blue curve is almost coincident with that retrieved on the bare laser A.<sup>[22]</sup> c) Intermode beatnote measured while driving the coupled laser system at a current of 550 mA. The shaded areas, labeled as I, II, III in panel b) identify different transport regimes in which the laser intracavity dynamics changes.

continuous range between 430 and 543 mA, then again over a small current portion (568–575 mA), and finally from 582 to 660 mA.

Overall the single beatnote persists over 30% of the laser dynamic range, i.e., over a region twice as wide as that retrieved in the bare laser A; this is a signature that the dispersion compensation induced by the polaritonic reflector allows phase locking of the lasing modes over a wider operational regime. A dual beatnote is then observed in the current range 543–568 mA, i.e., over a current portion slightly larger than that retrieved on the bare laser.<sup>[14]</sup> Such a regime reflects the dual comb nature of our heterogenous active core, with the two families of optical modes centered at  $\approx 3.1$  and  $\approx 2.7$  THz (Figure 3b–d) clearly visible at low driving currents. Finally, at currents larger than 660 mA we observe a broad beatnote, which is the signature of a lasing regime where the GDD is large enough to prevent the FWM from locking the lasing modes, in both frequency and phase, simultaneously.

The comparison between the FTIR spectra of the bare laser A (Figure 3c,e) and those of the coupled laser system (Figure 3b,d) do not reveal any visible change both in the regime where the coupled system shows a single beatnote (Figure 3b,c) and in the high current regime, dominated by dispersion (Figure 3d,e). Conversely, the comparison between the corresponding beatnotes (Figure 4a) clearly shows the efficacy of the proposed approach. At  $I_A = 650$  mA, a single, 30 dBm intense RF signal is retrieved, while the bare laser A shows a very broad beatnote.<sup>[14]</sup>

To confirm that the measured phenomena are correctly ascribed to the ISB polaritonic grating, we repeat the same experimental procedure after turning the polaritonic absorber by  $90^\circ$ , so that the polarization of the incoming THz beam is unable to activate ISB transitions in the MQW grating structure (s-polarization). In this configuration, which basically corresponds to the case of a reflecting gold grating (the ISB absorption is strongly suppressed<sup>[26]</sup>), the beatnote spectrum remains unaltered with respect to that of the bare laser.<sup>[14]</sup> The analysis of the beatnote LW across the current dynamic range of laser A coupled to the polaritonic mirror in the p- and s-polarized cases is shown in Figure 4b. We evaluate the beatnote LW by fitting the acquired RF spectra with a Lorentzian distribution (in the case of single

beatnote) or by determining the half-width-at-half-maximum (HWHM) of the power spectral density distribution (in the cases of broad beatnote). The coupling with the polaritonic mirror (p-polarization) efficiently reduces the intermode beatnote LW over the whole laser dynamic range, with respect to the case of a QCL coupled with a gold grating double metal cavity (s-polarization), which conversely does not induce any change on the intermode beatnote LW with respect to the case of the bare laser.<sup>[22]</sup> At currents  $I_A < 543$  mA (region I, Figure 4b), the RF spectrum shows a single narrow beatnote for both p- and s-polarizations, meaning that laser A is behaving like a comb, regardless of the coupling configuration adopted. Such an effect is expected since, even if the ISB transition is not activated, the polaritonic grating is here behaving as a gold-like reflector which, when in the “on-resonance” GTI configuration<sup>[22]</sup> ( $d_c \sim 50$   $\mu\text{m}$ ), is expected to compensate the QCL GDD, although over a partial frequency window (2.7–3.1 THz), as we experimentally demonstrated on the same laser bar.<sup>[22]</sup> However, once coupling the QCL with the polaritonic mirror (p-polarization), the LW is significantly reduced by more than a factor of five, reaching a minimum of 760 Hz at  $I_A = 550$  mA (Figure 4c).

This result is explained by the simulation of Figure 2a, which shows that the reflectivity of the ISB polaritonic mirror induces a reduction of the total GDD with respect to that of the bare laser A over a wider spectral window (2.55–3.15 THz), matching 80% of the spectral emission of the coupled system (Figure 3b). The LW of the main beatnote (even when a double beatnote appears) remains  $< 850$  Hz until a driving current of 582 mA. Above 582 mA neither the bare QCL nor the QCL coupled to the s-polarized mirror presents an individual narrow beatnote. This means that the group velocity dispersion is sufficiently strong to break the intermode coherence generated by the intracavity FWM process<sup>[14]</sup> and that the GTI comprising the gold grating structure even in the on-resonance condition is unable to compensate dispersion. The latter effect is in full agreement with previous experimental reports.<sup>[22]</sup> However, in the coupled system comprising the QCL and the polaritonic mirror in p-polarization, at 582 mA, the narrow individual beatnote regime persists, which is signature of the fact that the GDD is compensated by the modulation of the losses induced by the polaritonic mirror. This is reflected in the

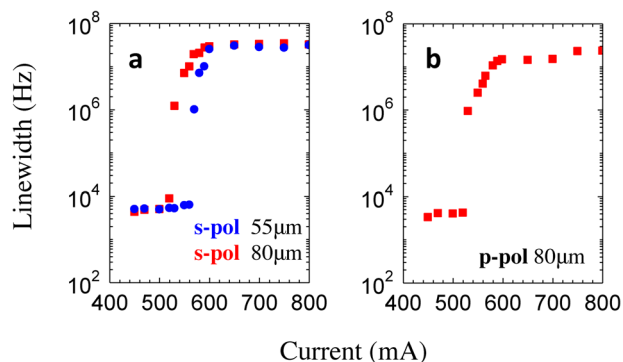


**Figure 5.** a) Intermode beatnote linewidth plotted as a function of the driving current of laser A coupled with the polaritonic mirror under s-polarization and while placing the polaritonic mirror at 55 μm distance or at 80 μm distance from the back QCL facet. b) Intermode beatnote linewidth plotted as a function of the driving current of laser A coupled with the polaritonic mirror under p-polarization and while placing the polaritonic mirror at 80 μm distance from the back QCL facet.

simulation results (Figure 2b) which show that, at 580 mA, the total GDD is drastically reduced and compensated over a spectral window extending from 2.55 to 3.2 THz, i.e., matching almost the whole emission bandwidth of the QCL (Figure 2b). At driving currents in the range 582–660 mA (region II, Figure 4b), the beatnote LW slightly increases (900 Hz to 7 kHz) as a consequence of the predicted GDD increase (Figure 2c), but remains single, confirming the prediction of the simulations (Figure 2c). The latter indeed show that the total GDD of the integrated QCL-polaritonic mirror system remains lower than the GDD of the bare laser over a slightly smaller spectral window 2.58–3.1 THz.

Finally, at currents larger than 660 mA (region III), the beatnote becomes wider. Interestingly, a visible reduction of the phase noise (by more than one decade) is observed. In contrast, the GTI comprising the QCL and the gold-grating double metal cavity (s-polarization) does not show any beatnote for any current value in the 550–1050 mA range (Figure 4b, regions II and III).

To further confirm our claim that the GDD is sensibly compensated by the modulation of the losses induced by the polaritonic mirror, we repeat the same experiment by varying the distance between the polaritonic mirror and the QCL back facet under both polarizations (p-pol and s-pol). First, we slightly detun (by 5 μm) the position of the mirror and collect the bias-dependent intermode beatnote under the polarization state where ISB absorption is not activated (s-pol). The intermode beatnote linewidth remains practically unperturbed with respect to the bare laser case (see Figures 4c and 5), confirming that the mirror is here behaving as a simple gold mirror in an on-resonance GTI configuration, in complete agreement with previous reports.<sup>[22]</sup> We then vary the distance of the polaritonic mirror up to 80 μm, therefore defining an off-resonance GTI.<sup>[22]</sup> We collect the beatnote map under both polarizations (Figure 5). The results clearly show that no dispersion compensation is achieved either in p-pol or in s-pol configurations, meaning that the off-resonance GTI is ineffective to induce a visible dispersion compensation either in the case of light-activated ISB transitions, or when the mirror is behaving as a simple gold grating.<sup>[22]</sup>

In addition to GDD compensation, the coupling with the nonlinear polaritonic mirror also induces non negligible effect in the QCL cavity with respect to designs relying solely on incoherent absorption. Strong-field excitation by single-cycle THz waveforms recently unveiled coherent nonlinear dynamics in the employed polaritonic grating,<sup>[26]</sup> including four-wave and six-wave mixing processes, which lead to a transient collapse of light-matter coupling on sub-cycle time scales.<sup>[26]</sup> The retrieved FWM and six-wave mixing nonlinearities might contribute to FC stabilization through the same mechanism as the fast saturable gain in the QCL AR, forcing the THz QCL into frequency-modulated operation.<sup>[31]</sup>

We then couple the polaritonic mirror with laser B. We first characterize the spectral behavior of the bare laser. By spanning the driving current  $I_B$ , over the whole dynamic current range, i.e., from 200 mA (threshold current) to 490 mA (roll-off current), we find four distinct lasing regimes. The laser is initially single mode (emitting at 3.23 THz) for  $I_B < 210$  mA (Figure 6a). Then, up to  $I_B = 270$  mA, only the higher-frequency stage of the heterogenous active medium is above threshold, with modes separated by the cavity round-trip frequency  $f_{rt} = 17.0$  GHz (Figure 6b). In this regime, the RF spectrum shows a single and narrow beatnote at  $\approx 17$  GHz; the intermodal frequency varies from 16.2 GHz at  $I_B = 210$  mA to 17.5 GHz at  $I_B = 270$  mA, with LW  $\sim 20$  kHz (Figure 6e). At higher  $I_B$  (between 270 and 320 mA), the lower-frequency AR module crosses threshold. In this range, the QCL operates in an harmonic state,<sup>[17,32–34]</sup> where the spacing between adjacent modes is  $2f_{rt}$  for the higher frequency AR module, whereas it is equal to  $6f_{rt}$  for the lower frequency module (Figure 6c). This regime is driven by the interplay of the third-order population pulsation (PP) nonlinearity and the population grating (PG) induced in the cavity by the primary mode of the lower frequency AR,<sup>[32]</sup> the intense mode at 2.73 THz in Figure 6c. Basically, this single-mode instability is the result of the standing-wave of the primary mode, which induces a spatial modulation of the population inversion (spatial hole burning), whose interaction with adjacent optical modes can suppress neighboring Fabry–Perot modes, while favoring sidebands that are some (or several)  $f_{rt}$  apart. The third-order nonlinearity of the active medium can simultaneously give rise to a temporal modulation of the population inversion. As a result of the PP and PG combination, the QCL shows a beatnote, which can be the signature of an amplitude modulation (AM) of the THz wave in the time domain if the PP effect is dominant or of a frequency modulation (FM) when the PG is dominant. We argue that in our device both mechanisms are simultaneously present.<sup>[28]</sup>

The RF spectrum in this regime is characterized by a narrow beatnote at a frequency  $2f_{rt}$ . Our experimental arrangement does not allow us to determine whether there is another beatnote at  $6f_{rt}$ , and no beatnote is observed at 17 GHz. The RF spectrum is shown in Figure 6f, with a stable and narrow beatnote with LW  $\approx 8$  kHz, demonstrating the coherence of the adjacent modes in the high frequency portion of the spectrum. It is worth mentioning that laser A is never driven in a stable harmonic comb state, but at a driving current  $I_A = 512$  mA we observe emission with spacing between adjacent modes of  $4f_{rt}$  for the lower frequency AR module, whereas it is equal to  $f_{rt}$  for higher frequency module (Supporting Information).

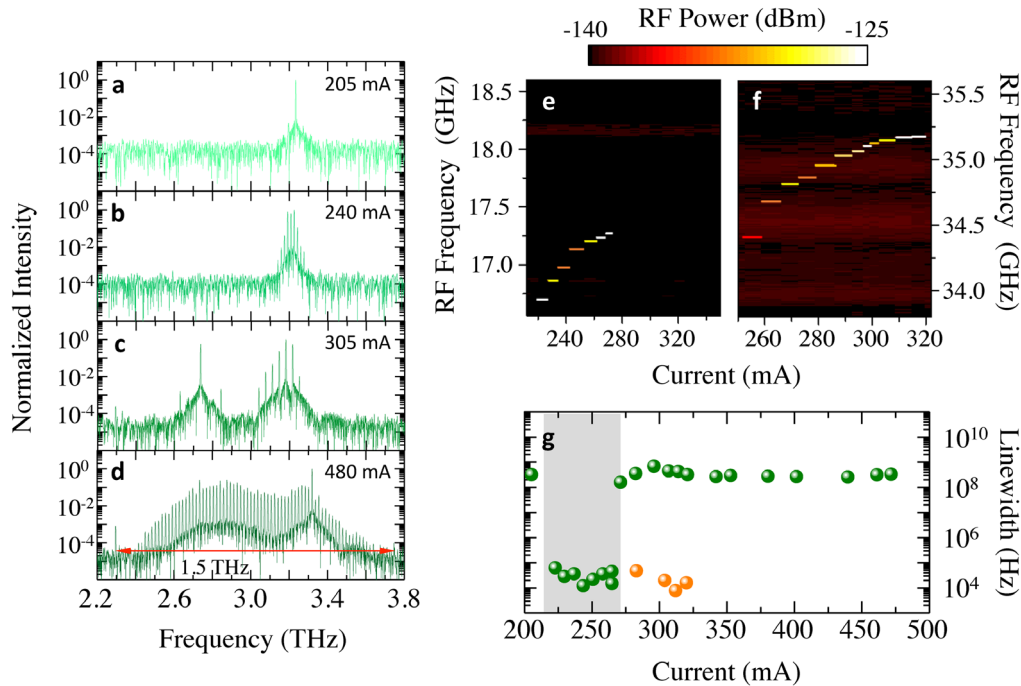


**Figure 6.** Spectral characterization and intermode beatnote spectroscopy of laser B. a–d) FTIR emission spectra of the bare laser B, recorded at  $T_H = 15$  K and at driving currents of a) 210 mA, b) 240 mA, c) 305 mA, and d) 480 mA. e) Intermode RF spectrum recorded in the range  $210 \text{ mA} < I_B < 335 \text{ mA}$ ; f) beatnote map recorded when laser B is operated in the harmonic comb regime ( $260 \text{ mA} < I_B < 325 \text{ mA}$ ), showing a visible peak at  $\approx 35$  GHz. For a small current range  $260 \text{ mA} < I_B < 270 \text{ mA}$ , the beatnotes at 17 and 34 GHz coexist. g) Intermode beatnote linewidths plotted as a function of the driving current (green dots indicate the standard FC, orange dots indicate the harmonic state). The gray shaded area shows the region in which the device behaves as an FC, showing a single, narrow beatnote.

For  $I_B > 320$  mA, all the modules of the heterogenous AR are activated and a broad (1.5 THz, with a continuous sequence of equally spaced optical modes covering 1.38 THz) and dense spectrum is observed up to  $I_B = 480$  mA (Figure 6d), corresponding to an emitted optical power of 7.2 mW. In this regime, dominated by cavity dispersion, a broad beatnote is retrieved, which is the signature of the lack of phase coherence between the lasing modes. The plot of the  $f_{rt}$  beatnote linewidths (Figure 6g) shows that laser B is behaving as a stable FC over a dynamic current range ( $\Delta I_B$ ) = 15%.

We then couple laser B with the polaritonic mirror, at a distance of 50  $\mu\text{m}$ , both in the conventional orientation (p-polarization) and in the s-polarization configuration where the ISB transition in the polaritonic region cannot be activated. The comparison between the intermode beatnote maps (Figure 7a,d) shows that, in the s-polarized case, the behavior of the QCL approximately matches that of the bare laser B, with a single beatnote persisting in the 220–275 mA range. The beatnote LW values are also comparable ( $\approx 10$  kHz) with those found in the bare laser B (Figure 6g). Similarly to what happens in the case of the bare laser B, when  $I_B$  is driven above 270 mA, the QCL shows 15 optically active modes separated by  $2f_{rt}$  (Figure 7f). At currents larger than 270 mA, the laser does not behave as a comb over the remaining current dynamic range.

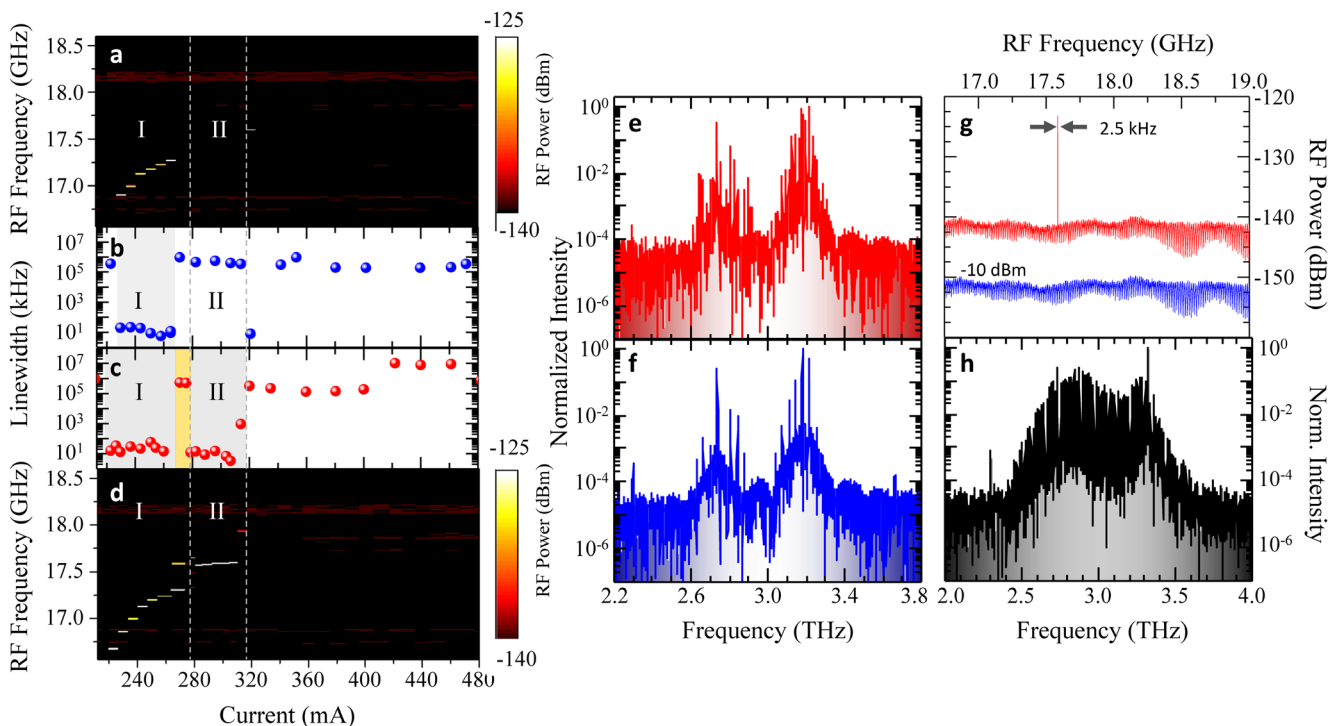
The picture drastically changes when the polaritonic mirror is integrated with the QCL, with the opposite coupling geometry (p-polarization). The intermode beatnote map shows an individual narrow (LW  $\sim 10$  kHz) beatnote for  $I_B < 270$  mA, as shown in

Figure 7c,d. A second beatnote (at 17.6 GHz) appears in a very small current range (275–280 mA), just above the onset of laser action of the second AR. This is a signature of the persistence of a dual-comb operational regime, in which the two AR stacks are individually locked in phase with slightly detuned intermode frequencies, although not phase-locked together.

Then, for  $280 \text{ mA} < I_B < 320 \text{ mA}$ , the beatnote returns again to be single and narrow (2.5–8 kHz) and a large number of lasing modes (40), spectrally spaced at  $f_{rt}$ , appear (Figure 7e); therefore, the polaritonic mirror allows the laser to be driven from a harmonic comb state (Figures 6c) to a phase-stabilized FC. Correspondingly, a visible intermode beatnote LW reduction down to 2.5 kHz at  $I_B = 305$  mA is detected (Figure 7g). This result is ascribed to the nontrivial response of the polaritonic mirror to the amplitude modulation of the harmonic comb output. The optical feedback from a simple reflector, such as the s-polarized grating or a gold mirror is insufficient to compensate the single-mode instability that drives the laser in the harmonic state. On the other hand, the strong compensation of the GDD induced by the p-polarized polaritonic mirror is capable of preventing the instability from taking place. In this regime, simulations predict a visible reduction of the GDD (see Figure S1b, Supporting Information).

Finally at  $I_B = 320$  mA, when the third stage of the AR (centered at 3.0 THz) reaches the lasing threshold, the single beatnote frequency abruptly shifts to 17.9 GHz, while still preserving its narrow nature. For currents  $> 320$  mA, the coherence between the modes is lost and a broad beat note (LW  $> 100$  MHz) is observed, in agreement to what predicted by simulations (see





**Figure 7.** Spectral characterization and intermode beatnote spectroscopy of the integrated laser system. a) RF beatnote map recorded as a function of the driving current when the polaritonic mirror is positioned at the QCL back-facet in s-polarization. b) Beatnote LW for coupling under s-polarization. The gray shaded area indicates the regime of stable comb operation. c) Beatnote LW for coupling under p-polarization; and d) corresponding beatnote map. The comb operation is extended over the current range 270–320 mA. The transition from the lower FC current range (region I) to the higher FC current range (region II) is marked by the presence of two narrow beatnotes at 17.3 and at 17.6 GHz (yellow shaded area, in panel (c)). e, f) THz spectra recorded at  $T_H = 15$  K, while driving the QCL in CW with a current of 305 mA for e) p- and f) s-polarization states. g) Stacked RF spectra measured while driving the QCL in CW with a current of 305 mA for the p- (red trace) and s- (blue trace) polarization states. h) FTIR spectrum recorded in CW at  $I_B = 480$  mA, while keeping  $T_H = 15$  K.

the Supporting Information). The corresponding laser spectrum (Figure 7h) shows 80 optically active modes, covering a bandwidth of 1.25 THz (2.3–3.55 THz).

Remarkably, the integration with the polaritonic mirror leads to an overall increase of the comb dynamic range operation from 13% in the case of the bare laser to  $\approx 30\%$ , in full agreement with that measured with laser A. As a common characteristic between laser A and B, when coupling of the QCL back facet with a reflector having a frequency and light-intensity dependent reflectivity, the optical power emitted by the integrated QCL comb increases by 35% in both lasers, reaching a maximum value of 5.5 mW in laser A and 8.1 mW in laser B.

#### 4. Conclusions

In conclusion, we demonstrate that by engineering an ISB polariton saturable absorber reflector, with dynamics considerably faster than the gain recovery time of QCLs,<sup>[27]</sup> and by coupling it with broadband THz QCLs, stable optical FCs are generated, characterized by narrow free running intermode beatnote LWs (700 Hz) and up to 8 mW of emitted optical power, spread over  $\geq 40$  teeth. We show that the polaritonic mirror behaves as a novel and efficient dispersion compensator of the complex gain profile of a heterogenous QCL. As a future perspective, the presented ISB polaritonic mirror can be eventually electrically driven to

exploit a further tuning of the GTI GDD via the quantum Stark effect.

Further, as the polaritonic mirror can simultaneously act as a saturable absorber mirror,<sup>[27]</sup> our experimental results can potentially open a path toward passively THz mode-locked microcavity lasers in a monolithic single-chip design with wide implications for: metrology, where laser excitation can match the energy levels splitting of molecules and its pulsed nature can down-convert the spectrum to the RF domain; ultrafast communications, where THz frequency carriers are requested for high-bandwidth data transfer; and, THz quantum optics, where high-power pulses can drive molecular samples out of equilibrium.

#### 5. Experimental Section

**QCL Fabrication:** The QCL was processed in a double-metal configuration starting from Au–Au (400 nm/400 nm) wafer bonding via thermo-compression on a highly doped GaAs carrier (or receptor) wafer. The bottom highly doped GaAs contact layer was then exposed through a combination of mechanical thinning and selective wet-etching, after removing the  $Al_{0.5}Ga_{0.5}As$  etch-stop layer. The 17  $\mu m$  thick AR was then defined by dry etching in an inductively coupled plasma reactive ion etching facility. Dry etching allowed almost vertical sidewalls, which resulted in uniform current injection and reduced lateral optical scattering. A Cr(10 nm)/Au(150 nm) top contact was then defined by a combination of optical lithography (SUSS MicroTec MJB4), thermal evaporation, and

lift-off. The top contact was intentionally patterned narrower than the ridge top surface, allowing thin nickel side-absorbers (setbacks) to be deposited via optical lithography on the uncovered portion of the ridge surface, using a laser writer (MicroWriter ML3 Durham Magneto Optics).<sup>[14]</sup> The side-absorbers were 5  $\mu\text{m}$  wide and 5 nm thick for laser A, and 2  $\mu\text{m}$  wide and 5 nm thick for laser B. Laser bars were finally cleaved, mounted on a copper bar with an indium-based thermally conductive adhesive paste, wire bonded with an ultrasound wedge bonding and connected to high frequency coplanar waveguides.

## Supporting Information

Supporting Information is available from the Wiley Online Library or from the author.

## Acknowledgements

This work was partially supported by the European Research Council through the ERC Grant 681379 (SPRINT), the European Union FET open project ULTRAQCL (665158), and by the EPSRC (UK) programme 'Hyper-Terahertz (EP/P021859/1). E.H.L. acknowledges support of the Royal Society and Wolfson Foundation.

## Conflict of Interest

The authors declare no conflict of interest.

## Data Availability Statement

The data that support the findings of this study are available on request from the corresponding author. The data are not publicly available due to privacy or ethical restrictions.

## Keywords

frequency combs, intersubband polaritons, quantum cascade lasers, terahertz

Received: December 18, 2020

Revised: February 26, 2021

Published online:

- [1] A. Di Gaspare, L. Viti, H. E. Beere, D. D. Ritchie, M. S. Vitiello, *Nanophotonics* **2020**, *10*, 181.
- [2] F. Krausz, M. I. Stockman, *Nat. Photonics* **2014**, *8*, 205.
- [3] L. F. Mollenauer, P. V. Mamyshv, J. Gripp, M. J. Neubelt, N. Mamyshva, L. Grüner Nielsen, T. Veng, *Opt. Lett.* **2000**, *25*, 704.
- [4] L. Consolino, A. Taschin, P. Bartolini, S. Bartolini, P. Cancio, A. Tredicucci, H. E. Beere, D. A. Ritchie, R. Torre, M. S. Vitiello, P. De Natale, *Nat. Commun.* **2012**, *3*, 1040.
- [5] T. Udem, R. Holzwarth, T. W. Hänsch, *Nature* **2002**, *416*, 233.
- [6] T. W. Hänsch, *Rev. Mod. Phys.* **2006**, *78*, 1297.
- [7] F. Adler, K. C. Cossel, M. J. Thorpe, I. Hartl, M. E. Fermann, J. Ye, *Opt. Lett.* **2009**, *34*, 1330.

- [8] L. H. Li, L. Chen, J. Zhu, J. Freeman, P. Dean, A. Valvanis, A. G. Davies, E. H. Linfield, *Electron. Lett.* **2014**, *50*, 309.
- [9] Q. Lu, F. Wang, D. Wu, S. Slivken, M. Razeghi, *Nat. Commun.* **2019**, *10*, 2403.
- [10] M. S. Vitiello, L. Consolino, S. Bartolini, A. Taschin, A. Tredicucci, M. Inguscio, P. De Natale, *Nat. Photonics* **2012**, *6*, 525.
- [11] D. R. Bacon, J. R. Freeman, R. A. Mohandas, L. Li, E. H. Linfield, A. G. Davies, P. Dean, *Appl. Phys. Lett.* **2016**, *108*, 081104.
- [12] A. Hugi, G. Villares, S. Blaser, H. C. Liu, J. Faist, *Nature* **2012**, *492*, 229.
- [13] M. Rosch, G. Scalari, M. Beck, J. Faist, *Nat. Photonics* **2015**, *9*, 42.
- [14] K. Garrasi, F. P. Mezzapesa, L. Salemi, L. Li, L. Consolino, S. Bartolini, P. De Natale, A. G. Davies, E. H. Linfield, M. S. Vitiello, *ACS Photonics* **2019**, *6*, 73.
- [15] D. Burghoff, T.-Y. Kao, N. Han, C. Wang, I. Chan, X. Cai, Y. Yang, D. J. Hayton, J.-R. Gao, J. L. Reno, Q. Hu, *Nat. Photonics* **2014**, *8*, 462.
- [16] L. Consolino, M. Nafa, F. Cappelli, K. Garrasi, F. P. Mezzapesa, L. Li, A. G. Davies, E. H. Linfield, M. S. Vitiello, P. De Natale, S. Bartolini, *Nat. Commun.* **2019**, *10*, 2938.
- [17] A. Forrer, M. Franckić, D. Stark, T. Olariu, M. Beck, J. Faist, G. Scalari, *ACS Photonics* **2020**, *7*, 784.
- [18] P. Tzenov, D. Burghoff, Q. Hu, C. Jirauschek, *Opt. Express* **2016**, *24*, 23232.
- [19] J. B. Khurgin, Y. Dikmelik, A. Hugi, J. Faist, *Appl. Phys. Lett.* **2014**, *104*, 081118.
- [20] D. Burghoff, Y. Yang, D. J. Hayton, J. R. Gao, J. L. Reno, Q. Hu, *Opt. Express* **2015**, *23*, 1190.
- [21] Y. Yang, D. Burghoff, J. Reno, Q. Hu, *Opt. Lett.* **2017**, *42*, 3888.
- [22] F. P. Mezzapesa, V. Pistore, K. Garrasi, L. Li, A. G. Davies, E. H. Linfield, S. Dhillon, M. S. Vitiello, *Opt. Express* **2019**, *27*, 20231.
- [23] D. Dini, R. Köhler, A. Tredicucci, G. Biasiol, L. Sorba, *Phys. Rev. Lett.* **2003**, *90*, 116401.
- [24] Y. Todorov, C. Sirtori, *Phys. Rev. B* **2012**, *85*, 045304.
- [25] J. Raab, C. Lange, J. L. Boland, I. Laepple, M. Furthmeier, E. Dardanis, N. Dessmann, L. Li, E. H. Linfield, A. G. Davies, M. S. Vitiello, R. Huber, *Opt. Express* **2019**, *27*, 2248.
- [26] J. Raab, F. P. Mezzapesa, L. Viti, N. Dessmann, L. Li, A. G. Davies, E. H. Linfield, C. Lange, R. Huber, M. S. Vitiello, *Nat. Commun.* **2020**, *11*, 4290.
- [27] R. Houdré, J. L. Gibernon, P. Pellandini, R. P. Stanley, U. Oesterle, C. Weisbuch, J. O'Gorman, B. Roycroft, M. Ilegems, *Phys. Rev. B* **1995**, *52*, 7810.
- [28] D. Burghoff, Y. Yang, J. Reno, Q. Hu, *Optica* **2016**, *3*, 1362.
- [29] M. Wienold, L. Schrottke, M. Giehler, R. Hey, W. Anders, H. T. Grahn, *Electron. Lett.* **2009**, *45*, 1030.
- [30] F. Wang, H. Nong, T. Fobbe, V. Pistore, S. Houver, S. Markmann, N. Jukam, M. Amanti, C. Sirtori, S. Moumdji, R. Colombelli, L. Li, E. Linfield, G. Davies, J. Mangeney, J. Tignon, S. Dhillon, *Laser Photonics Rev.* **2017**, *11*, 1700013.
- [31] N. Henry, D. Burghoff, Q. Hu, J. Kurgin, *Opt. Express* **2010**, *18*, 20799.
- [32] T. S. Mansuripur, C. Vernet, P. Chevalier, G. Aoust, B. Schwarz, F. Xie, C. Caneau, K. Lascola, C. E. Zah, D. P. Caffey, T. Day, L. J. Missaggia, M. K. Connors, C. A. Wang, *Phys. Rev. A* **2016**, *94*, 063807.
- [33] D. Kazakov, M. Piccardo, Y. Wang, P. Chevalier, T. S. Mansuripur, F. Xie, C.-E. Zah, K. A. Lascola, A. Belyanin, F. Capasso, *Nat. Photonics* **2017**, *11*, 789.
- [34] F. Wang, V. Pistore, M. Riesch, H. Nong, P. B. Vigneron, R. Colombelli, O. Parillaud, J. Mangeney, J. Tignon, C. Jirauschek, S. S. Dhillon, *Light: Sci. Appl.* **2020**, *9*, 51.